

Enabling Polaritonic MEMS at room temperature with strongly coupled Tamm plasmon polaritons in metal/air-gap DBRs

C. Grossmann,^{1, a)} C. Coulson,¹ G. Christmann,¹ I. Ferrer,² H. Beere,² D.A. Ritchie,² and J. J. Baumberg¹

¹*Nanophotonics Centre, Cavendish Laboratory, University of Cambridge, Cambridge CB3 0HE, United Kingdom.*

²*Semiconductor Physics Group, Cavendish Laboratory, University of Cambridge, Cambridge CB3 0HE, United Kingdom.*

(Dated: 21 February 2011)

We report strong coupling between Tamm plasmons and excitons in III-V quantum wells at room temperature in an ultracompact sample design which can be electrically-tuned in real-time. A thin gold layer is deposited onto a two-pair AlGaAs/air-gap distributed Bragg reflector containing three GaAs quantum wells. The high refractive index contrast mirror together with optical Tamm states at the metal-semiconductor interface tightly confines the intracavity field leading to a substantial local field enhancement. Angular-resolved reflectivity spectra give clear evidence for anti-crossing in the dispersion relation, signalling the strong-coupling regime. Rabi splittings of 10 meV at room temperature are found in excellent agreement with simulations. Electrical control of the polariton modes is realized without need for doped mirror layers. Such air-gap microcavities open new possibilities for electrically-tunable microcavities and polaritonic micro-electromechanical effects.

In a strongly-coupled semiconductor microcavity, the cavity photon and exciton modes form coherent coupled states termed cavity polaritons that have partly photonic and partly excitonic character. These quasiparticles possess new properties which allow observation of polariton condensation,^{1,2} stimulated scattering,³ quantized vortices⁴ or superfluid behaviour.⁵ Besides their fundamental physics, polaritons have possible applications in ultrafast optical switches,^{3,6} ultralow threshold polariton lasers^{7,8} or light emitting diodes⁹⁻¹¹. While most results so far are obtained at cryogenic temperatures great efforts have been made to realize stable polaritons at room temperature, which require the light-matter interaction energy to be comparable to the thermal energy.

The strength of this exciton-photon coupling is characterized by the vacuum Rabi splitting energy $\hbar\Omega_R$ which depends on the oscillator strength of the excitonic transition and the electromagnetic field amplitude at the quantum well (QW) position, which can be separately optimised.¹² Excitons with large binding energy and oscillator strength in GaN-¹³ or ZnO-based¹⁴ semiconductors can be used in planar microcavities, enabling strong coupling at room temperature. However these structures suffer from lower optical quality and electrical performance than III-V structures which remain the paradigm system at lower temperatures. Organic semiconductors show even larger exciton binding energies¹⁵ but their lifetime is limited by irreversible bleaching. Increasing the numbers of QWs and mirror layers maximizes the oscillator strength and cavity Q-factor, allowing strong coupling at elevated temperatures in III-V microcavities.^{16,17}

An alternative approach to increase the exciton-photon coupling is to confine the optical mode more tightly. A

shorter effective cavity length (including mirror penetration) L_{eff} produces a higher Rabi splitting, $\hbar\Omega_R \propto 1/\sqrt{L_{eff}}$.¹² This concept was demonstrated in microcavities with AlO_x/GaAs distributed Bragg reflectors (DBRs) where strong-coupling at room temperature was first observed¹⁸. Thanks to an even larger large refractive index contrast, air-gap DBRs composed of alternating air and dielectric layers show peak reflectivities of 99.9% across a stopband of many hundred nanometers with only two pairs of mirror layers.¹⁹ In conjunction with optical Tamm states which are localized photon modes at a metal/DBR interface,^{20,21} this enables the generation of large field amplitudes at the QW position located just beneath the metal interface.

Here we show experimental evidence of strong coupling between Tamm plasmons and GaAs excitons at room temperature in a simple 5-layer sample design. The building blocks of our structure are a two-layer air-gap DBR, three GaAs QWs and a metal interface which supports the optical Tamm modes and completes the cavity. This approach allows the study of confinement effects in three dimensions as well as introduces an additional degree of freedom to investigate acoustic and electro-mechanical coupling of polaritons. Furthermore such miniaturisation enables integrated devices operating under plausible conditions for applications.

The MBE-grown structure (Fig.1a) consists of an Al_{0.1}Ga_{0.9}As/AlAs multilayer stack of respective thickness 184nm/212nm, forming the DBR. Three 100Å thick GaAs QWs with Al_{0.1}Ga_{0.9}As barriers are embedded in an 86 nm thick spacer on top of the DBR. Air-gaps are created using a rectangular etch window defined by standard UV photolithography followed by reactive ion etching (RIE) in SiCl₄ to gain access to the buried AlAs layers (Fig.1b). A sacrificial wet etch process in 1% hydrofluoric acid selectively removes the AlAs and a two layer air-gap DBR is formed. The semiconductor layers have a thick-

^{a)}Electronic mail: cg439@cam.ac.uk

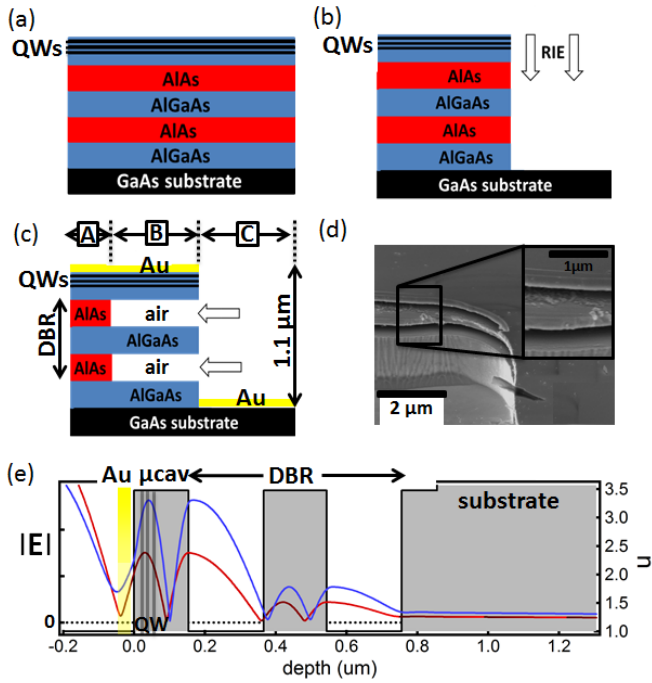


FIG. 1. Sample fabrication: (a) layer structure, (b) RIE etch, (c) sacrificial wet etch of AlAs layers, and (d) SEM of fabricated air-gaps. (e) Optical field distribution both with (blue line) and without (red line) gold layer, refractive index profile (black line).

ness of $\frac{3}{4}\lambda$ to increase their mechanical stability (Fig.1c). A critical point dryer is used to ameliorate the effects of surface tension and stiction as in standard micromechanical processing, and a 15 nm layer of gold is evaporated on top. In order to apply an electric field across the multilayer, wire-bonded contacts are fabricated onto the Au layers both on top of the mesa and on the GaAs substrate. In the scanning electron microscope (SEM) image (Fig.1d) the two air-gaps forming the bottom DBR are clearly visible.

The field enhancement at the QWs in the air-gap DBR sample due to the localized optical Tamm modes is clearly resolved in the calculated electromagnetic field distribution (Fig.1e). The optical field at the QWs doubles in the presence of the Au layer compared with the bare DBR structure. The strong confinement of the optical field is indicated by the short penetration depth ($<500\text{nm}$) into the air-gap mirror. These two effects influence the light-matter coupling beneficially.

The underetching across areas of several hundreds of μm^2 is clearly seen in bright-field microscope images (Fig.2a). Three areas with distinct colours are identifiable: the GaAs substrate (C), the underetched area (B) and the unprocessed wafer (A). The etch front of the sacrificial etch is clearly visible as the boundary between (A) and (B) and the uniform coloration of the processed area indicates a high degree of flatness of the suspended layers with few structural collapses or cracks. The etch

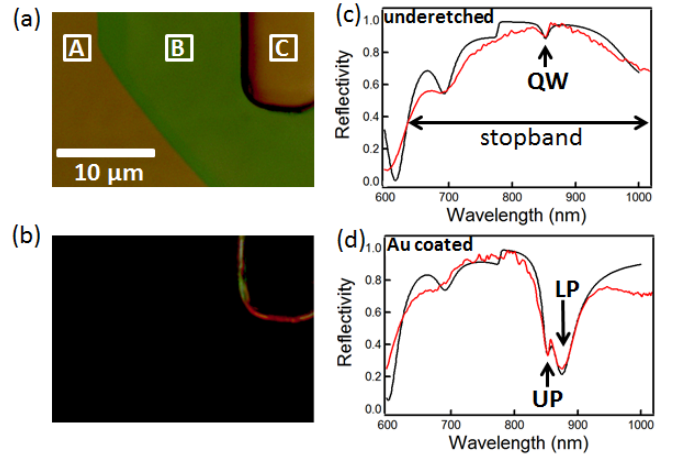


FIG. 2. Bright field (a) and dark field (b) images of underetched microcavity: (A) unprocessed area, (B) underetched area, (C) GaAs substrate. (c,d) (color online) Measured (red line) and calculated (black line) reflection spectra of underetched sample before (c) and after (d) Au coating.

anisotropy is due to the crystallographic orientation of the sample. The vertical mesa edge from the RIE process accounts for the strong scatter signal in the dark-field image of Fig.2(b), but shows no other defects.

Reflectivity spectra of the structure are measured at room temperature before the metal layer is evaporated (Fig.2c). A modified microscope with confocal detection under $\times 100$ magnification provides a measurement spot size of $6\mu\text{m}$ diameter. The DBR stopband (Fig.2c) exceeds 200nm width with 95% peak reflectivity, while the QW exciton shows a reflectivity dip at 854nm with a linewidth of 15meV at room temperature. The two minima at higher energy correspond to a cavity mode in the AlGaAs DBR layer (690nm) and the first reflectivity minimum of the stop-band edge of the DBR (620nm). The weak step in reflectivity at 780nm is caused by absorption in the AlGaAs barrier layers and confirms the strong field localisation in the cavity layer. We note the good agreement with transfer matrix simulations. After the Au upper mirror is evaporated, the QW absorption increases 8-fold and a second dip appears on its lower energy side (Fig.2d). This Tamm plasmon at 878nm exhibits a linewidth of 20meV , broader than the QW mode because it experiences absorption in the metal. As before, agreement with transfer matrix calculations is good.

In order to investigate the interaction between the QW excitons and the Tamm plasmon, angular-resolved reflectivity measurements are performed. A fibre-coupled white light source illuminates the sample through a microscope objective of high numerical aperture ($\text{NA}=0.9$). All the Tamm modes with wavevector $k = 0$ to $k_{max}=5\mu\text{m}^{-1}$ (limited by the NA) are simultaneously excited. The angles of incidence are selected in collection by spatially scanning the reflected parallel beam from the backside of the objective onto a $200\mu\text{m}$ core fibre coupled

into a spectrometer giving 4° resolution. We separately calibrate the angle of detection which varies from 0° to 45° .

A set of TE-polarized reflectivity spectra for a typical underetched region (Fig.3a) clearly show the Tamm mode shifting to higher energies for increasing angles of incidence, approaching the QW exciton line at 854nm. For angles greater than 40° , the energy shift saturates and the QW dip moves away from the Tamm mode. This anticrossing behaviour is a clear signature of strong coupling between the Tamm plasmon and the QW exciton which form new quasiparticles, the upper (UP) and lower (LP) polariton. Extracting the mode energies (Fig.3b) allows comparison with a standard polariton coupling model (which matches transfer matrix simulations) and resolves a Rabi splitting of $>10\text{meV}$. This value is larger than in other reports of strong coupling both at room temperature in GaAs-based structures^{16,22} and in Tamm plasmon polariton experiments carried out at liquid nitrogen temperature.²³ This arises from the $L_{eff} = 46\text{nm}$ penetration into the air-DBR compared to 560nm in conventional GaAs/AlAs designs.

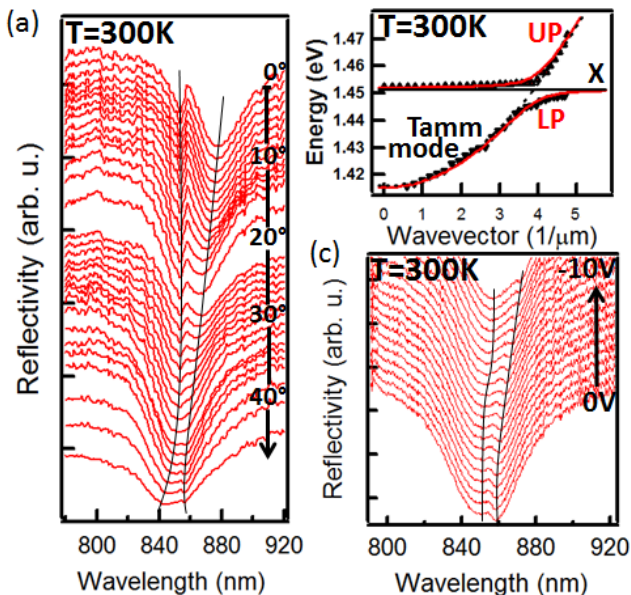


FIG. 3. (color online)(a) Angle-dependent reflectivity spectra. (b) Experimental dispersion curves (black triangles) and model (red line) of upper and lower polariton branches. The Tamm plasmon mode energy and the uncoupled exciton energy (X) are shown dashed. (c) Reflectivity spectra for applied bias from 0 to -10 V in steps of 0.5V (shifted for clarity).

The advantage of using air-spaced DBRs is the resultant tunability of such microcavity devices. Here we demonstrate the simplest operation mode by applying a vertical bias on the mesas from 0 to -10V. Reflectivity spectra (Fig.3c) clearly show bias tuning of the polaritons through the strong coupling anticrossing. Of the different tuning contributions which include the quantum-confined

Stark effect and electrostatic bending of the DBRs, the dominant contribution in the present contact geometry is from current heating of the mesa which red-shifts the exciton.

In conclusion, we successfully fabricate air-gap DBR microcavities which show strong coupling of Tamm plasmons and QW excitons at room temperature. The high-contrast DBRs and field-enhancement from the optical Tamm modes elicits Rabi splittings of $>10\text{ meV}$ with only three GaAs QWs, ten times fewer than in previous work at liquid nitrogen temperature.²³ These extremely compact devices with few layers simplify MBE growth tolerance and uniformity requirements and can be further optimised for instance by using $\frac{1}{4}$ DBR thicknesses and exploring lateral polariton confinement and transport. Bias tuning of polaritons is realized without the need for doped DBR layers, paving the way for electrically-controlled polaritons at room temperature in ultra-compact sample geometries based on well-established GaAs technology. This points the way towards applications in electrically-driven polariton lasers²⁴, Bose-Einstein condensation as well as exploiting MEMS and acoustic polariton devices.

The authors acknowledge financial support from UK EPSRC EP/C511786/1, EP/F011393 and EU CLERMONT4.

- ¹J. Kasprzak, M. Richard, S. Kundermann, A. Baas, P. Jeambrun, J.M.J. Keeling, F.M. Marchetti, M.H. Szymanska, R. Andre, J.L. Staehli, V. Savona, P.B. Littlewood, B. Deveaud, and Le Si Dang, Nature **443**, 409 (2006).
- ²R. Balili, V. Hartwell, D. Snoke, L. Pfeiffer, and K. West, Science **316**, 1007 (2007).
- ³P. G. Savvidis, J. J. Baumberg, R. M. Stevenson, M. S. Skolnick, D. M. Whittaker, and J. S. Roberts, Phys. Rev. Lett. **84**, 1547 (2000).
- ⁴K. G. Lagoudakis, M. Wouters, M. Richard, A. Baas, I. Carusotto, R. Andre, D. Le Si Dang, and B. Deveaud-Pledran, Nature Physics **4**, 706 (2008)
- ⁵A. Amo, D. Sanvitto, F. P. Laussy, D. Ballarini, E. del Valle, M. D. Martin, A. Lemaître, J. Bloch, D. N. Krizhanovskii, M. S. Skolnick, C. Tejedor, and L. Vina, Nature **457**, 291 (2009).
- ⁶T. C. H. Liew, A. V. Kavokin, and I. A. Shelykh, Phys. Rev. Lett. **101**, 016402 (2008).
- ⁷A. Imamoglu, R.J. Ram, S. Pau, and Y. Yamamoto, Phys. Rev. A **53**, 4250 (1996).
- ⁸S. Christopoulos, G. Baldassarri Höger von Högersthal, A. J. D. Grundy, P. G. Lagoudakis, A. V. Kavokin, J. J. Baumberg, G. Christmann, R. Butté, E. Feltn, J.-F. Carlin, and N. Grandjean, Phys. Rev. Lett. **98**, 126405 (2007).
- ⁹D. Bajoni, E. Semenova, A. Lemaître, S. Bouchoule, E. Wertz, P. Senellart, and J. Bloch, Phys. Rev. B **77**, 113303 (2008).
- ¹⁰A. A. Khalifa, A. P. D. Love, D. N. Krizhanovskii, M. S. Skolnick, and J. S. Roberts, App. Phys. Lett. **92**, 061107 (2008).
- ¹¹S. I. Tsintzos, N. T. Pelekanos, G. Konstantinidis, Z. Hatzopoulos, and P. G. Savvidis, Nature **453**, 372 (2008).
- ¹²M.S. Skolnick, T.A. Fisher, and D.M. Whittaker, Semi. Sci. Tech. **13**, 645 (1998).
- ¹³G. Christmann, R. Butte, E. Feltn, A. Mouti, P.A. Stadelmann, A. Castiglia, J.-F. Carlin, and N. Grandjean, Phys. Rev. B **77**, 08531019 (2008).
- ¹⁴R. Schmidt-Grund, B. Rheinlnder, C. Czekalla, G. Benndorf, H. Hochmuth, M. Lorenz, and M. Grundmann, App. Phys. B **93**, 331 (2008).

- ¹⁵D. G. Lidzey, D. D. C. Bradley, M. S. Skolnick, T. Virgili, S. Walker, and D. M. Whittaker, *Nature* **395**, 53 (1998).
- ¹⁶S. I. Tsintzos, P. G. Savvidis, G. Deligeorgis, Z. Hatzopoulos, and N. T. Pelekanos, *App. Phys. Lett.* **94**, 071109 (2009).
- ¹⁷J. Bloch, T. Freixanet, J. Y. Marzin, V. Thierry-Mieg, and R. Planel, *App. Phys. Lett.* **73** 1694 (1998)
- ¹⁸T.R. Nelson Jr., J.P. Prineas, G. Khitrova, H.M. Gibbs, J.D. Berger, J.-H. Shin, H.-E. Shin, Y.-H. Lee, P. Tayebati, and L. Javniskis, *App. Phys. Lett.* **69** 20 (1996)
- ¹⁹H. Hillmer, J. Daleiden, C. Prott, F. Roemer, S. Irmer, V. Rangelov, A. Tarraf, S. Schueler, and M. Strassner, *App. Phys. B* **75**, 3-13 (2002).
- ²⁰A. K. Kavokin, I. A. Shelykh, and G. Malpuech, *Phys. Rev. B* **72**, 233102 (2005).
- ²¹M. Kaliteevski, I. Iorsh, S. Brand, R. A. Abram, J. M. Chamberlain, A. V. Kavokin, and I. A. Shelykh, *Phys. Rev. B.* **76**, 165415 (2007).
- ²²R. Houdré, R. P. Stanley, U. Oesterle, C. Weisbuch, and M. Llegems, *Phys. Rev. B* **49**, 16761 (1994).
- ²³C. Symonds, A. Lemaitre, E. Homeyer, J. C. Plenet, and J. Bellessa, *App. Phys. Lett.* **95**, 151114 (2009).
- ²⁴A. K. Kavokin, I. A. Shelykh, and G. Malpuech, *App. Phys. Lett.* **87**, 261105 (2005).